Granular Fingering in Fluid Injection into Dense Granular Media in a Hele-Shaw Cell

Haiying Huang, Fengshou Zhang, and Patrick Callahan
School of Civil and Environmental Engineering, Georgia Institute of Technology, Atlanta, Georgia 30332, USA

Joseph Ayoub
Schlumberger, Sugar Land, Texas 77478, USA

(Received 23 February 2012; published 20 June 2012)

We study experimentally spontaneous pattern formation in a dry dense granular medium invaded by an aqueous glycerin solution in a radial Hele-Shaw cell. By varying the invading fluid viscosity via the weight concentration of glycerin, and by adjusting the normalized injection velocity via the injection rate and the gap size of the cell, we observe four distinct fluid-grain displacement regimes: (i) a simple radial flow regime, (ii) an infiltration-dominated regime, (iii) a grain displacement-dominated regime, and (iv) a viscous fingering-dominated regime. We argue that these displacement regimes emerge as a result of competition among the various energy dissipation mechanisms and can be classified based on the characteristic times involved in the injection process.

DOI: 10.1103/PhysRevLett.108.258001 PACS numbers: 45.70.Qj, 47.15.gp, 47.56.+r, 47.57.Gc

Complex patterns arise when a granular medium is invaded by a fluid. Extensive literature [1–4] exists for the two limiting uncoupled cases when the granular medium either behaves as a rigid porous medium or is submerged in a fluid to behave as a dilute suspension. When the grain displacements become coupled with fluid flow, ''granular fingering,'' an instability of Saffman-Taylor type, has been observed in experiments of air injection into granular media in Hele-Shaw cells [5–9]. The coupled fluid-grain displacement process is not only of fundamental scientific interest but also relevant to engineering applications such as ground improvement, environmental remediation, and reservoir stimulation.

In this Letter, we study the coupled fluid-grain displacement process when a dry dense granular medium is invaded by an aqueous glycerin solution in a radial Hele-Shaw cell. We demonstrate that there exists a transition from the solidlike to the fluidlike behaviors in the response of the dense granular medium. By varying the invading fluid viscosity via the weight concentration of glycerin, and by adjusting the normalized injection velocity via the injection rate and the gap size of the cell, we observe four distinct fluid-grain displacement regimes: (i) a simple radial flow regime, (ii) an infiltration-dominated regime, (iii) a grain displacement-dominated regime, and (iv) a viscous fingering-dominated regime.

The granular material used here is dry Ottawa F110 sand. The sand grain size is mostly in the range from 70 to 200 μm with the mean particle diameter by mass $d_p =$ 110 μm. The radial Hele-Shaw cell is made from two $305 \times 305 \times 25.4$ mm Plexiglass plates bolted together at the four corners, with the gap size, b, controlled by the metal spacers in between the two plates. Sand is rained into the Hele-Shaw cell when held in an upright position. The granular medium is compacted first by manual vibration during the filling stage and then on a vibration table after the cell is filled. The grain mass fraction obtained through such a sample preparation procedure is about 0.63 to 0.65. The outer boundary of the Hele-Shaw cell is sealed in all the tests to prevent decompaction near the boundary prior to and during the tests.

Aqueous glycerin solutions of three concentrations, 50%, 90%, and 100% concentration by weight, are used in the injection tests. The viscosity of the fluids measured at 21 °C is around 5, 176, and 942 cp, respectively. During the experiments, fluid is injected at the center of the bottom plate from a syringe pump at constant flow rates. High resolution images (3264×2456) are recorded using a Canon Vixia HFS100 HD camera placed on top of the cell. A summary of the test parameters is given in Table I for a series of 12 representative tests from a total of 58 tests. Tests A1-C4 are performed at four normalized injection velocities $v = Q/(\pi b D_i)$, where Q is the injection rate and $D_i = 1.016$ mm is the diameter of the injection inlet, while the remaining 46 tests are conducted at injection velocities selected from the range set by tests A1 and C4. We may assume that in these experiments, as far as fluid flow is concerned, the viscous effect instead of the capillary effect or the inertia effect is the dominant factor since in all the tests, the capillary number $\mathrm{Ca} = v\eta/\gamma > 10^{-5}$ ($\mathrm{Ca} = 6.52 \times 10^{-4}$ in test A1 and $\mathrm{Ca} = 6.58 \times 10^{-3}$ in test A2), assuming surface tension $\gamma = 0.063$ N/m for the glycerin solutions against air [10]. Meanwhile, if the Reynolds number is defined according to $\mathrm{Re} = \rho v b/\eta$, the largest Reynolds numbers are $\mathrm{Re} = 146.887$ in test A4 and $\mathrm{Re} = 58.755$ in test A3, assuming density $\rho =$ 1250 kg/m^3 for 100% glycerin. Fluid flow is therefore in the laminar regime.

The images from tests A1-C4 before the fluid fronts reach the cell boundaries are summarized in Fig. 1. The

 © 2012 American Physical Society

TABLE I. The invading fluid viscosity η and the normalized injection velocity v in tests A1-C4. The injection velocity v is adjusted through the injection rate Q and the gap size b of the Hele-Shaw cell. Tests A1-C1: $Q = 5$ ml/min, $b = 3.175$ mm; tests A2-C2: $Q = 25$ ml/min, $b = 1.575$ mm; tests A3-C3: $Q = 50$ ml/min, $b = 1.575$ mm; and tests A4-C4: $Q = 125$ ml/min, $b = 0.787$ mm.

Test Parameters	$\eta = 5$ cp	176 cp	942 cp
$v = 8.22$ mm/s	A1	B1	C1
82.90 mm/s	A2	B2	C2
165.80 mm/s	A3	B3	C3
829.52 mm/s	A4	B4	C4

light colored areas are occupied by dry sands only. The black areas indicate the fluid-only areas, and the brown areas are the fluid infiltrated areas. While fluid permeates through the granular medium with a nearly circular front and no fluid channels are created in test A1, in all other tests, fluid flow results in significant grain displacements, which in turn create channels occupied by fluid only. We may interpret the term "granular finger" in a broad sense and use it here to describe the fluid channels. As the

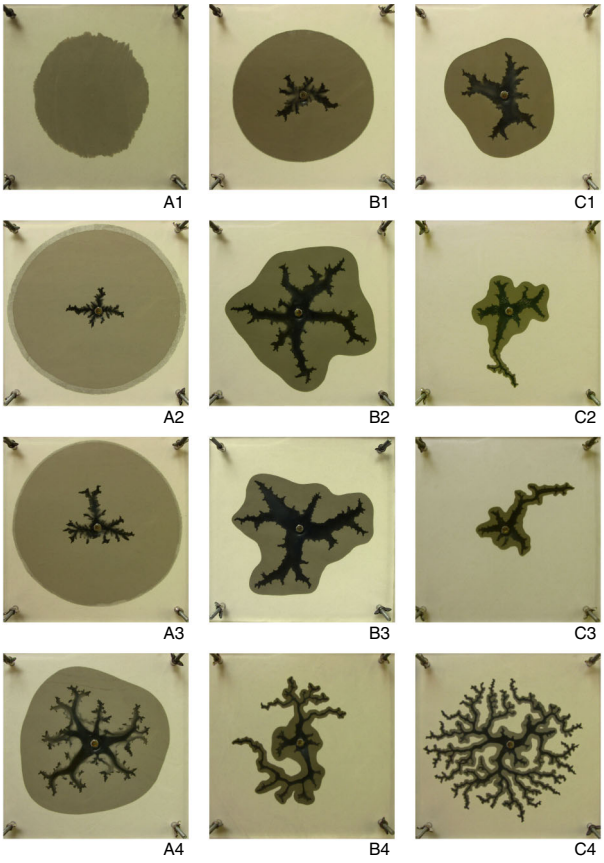

FIG. 1 (color online). Displacement patterns from the injection experiments with dry Ottawa F110 sand and aqueous glycerin solutions.

invading fluid viscosity and the injection velocity increases from test A1 to C4, we can identify a transition in the fluid flow behaviors from infiltration dominated to infiltration limited. Meanwhile, the response of the granular medium also changes from that of a rigid porous medium in test A1 to fluidlike in test C4 where the ramified finger morphology resembles the viscous fluid-fluid displacement pattern. In tests A2, A3, and B1, the permeation fronts remain nearly circular and are affected very little by the development of the granular fingers. In tests A4, B2, B3, C1, and C2, the permeation fronts reflect the propagation of the granular fingers, but not yet the development of individual granular fingers. The fingers grow much wider than those in tests A2, A3, and B1. In test C4, where the fluid viscosity and the injection velocity are the largest, the permeation front now closely follows individual granular fingers.

Since the velocity in the domain decreases with the radial distance, the effect of the relatively small Ca in test A2 is reflected by the narrow unsaturated outer zone that appears when the permeation front grows very close to the cell boundary. Meanwhile, due to the relatively large Re, evidences of erosion can be identified in test A4 from disconnected granular fingers and sloped finger perimeters. During all other tests, the finger perimeters remain sharp vertically. Test A4 is therefore excluded from further analysis.

Growth of the granular fingers with time from tests A2, B3, and C4 is shown in Figs. 2(a)–2(c). Figure 2(a) shows that fluid flow first creates a nearly circular cavity around the injection point. The circular shape then becomes distorted with time, eventually leading to the development of preferential paths. Growth of the fingers is mainly in the length direction in tests A2 and C4, but in both width and length directions in test B3. The fingers extend via tip blunting and splitting instead of side branching. The fractal dimensions of the granular fingering patterns, determined through box counting, decrease from around $D \backsimeq 1.73$ in tests A2, to 1.64 in test C4. Compared with the theoretical value of $D = 1.70 \pm 0.02$ for a diffusion-limited aggregation (DLA) pattern [11], the fractal dimension in test C4 is slightly smaller, likely due to the finite size and resolution of the image.

Based on the images in Fig. 1, we may classify the above tests into four displacement regimes, namely: (i) a simple radial flow regime (test A1), (ii) an infiltration-dominated regime (tests A2, A3, and B1), (iii) a grain displacement-dominated regime (tests A4, B2, B3, C1, and C2), and (iv) a viscous fingering-dominated regime (test C4). Tests B4 and C3 appear to be in the transition from the grain displacement-dominated regime to the viscous fingering-dominated regime. Emergence of these displacement regimes may be understood from the point of view of energy dissipation. The main energy dissipation mechanisms involved in this injection process are viscous dissipation through permeation in the granular medium, dissipation

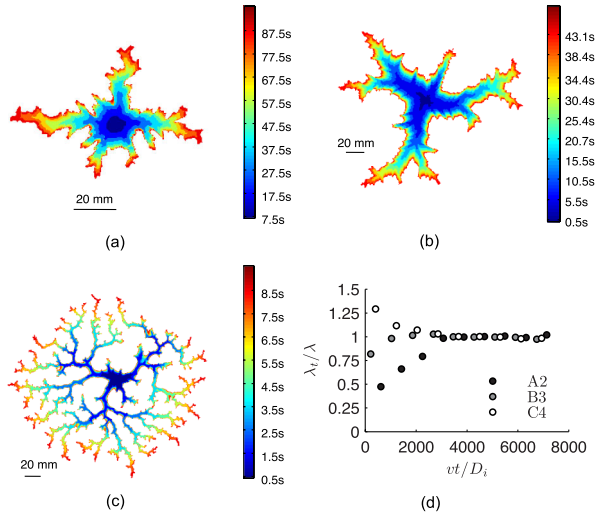

FIG. 2 (color online). Growth of the granular fingers with time from test A2 (a), B3 (b), and C4 (c), and variations of the normalized area ratio λ_t/λ with scaled time vt/D_i (d).

through grain displacements, and viscous dissipation for flow through the granular fingers. Therefore, competition among these energy dissipation mechanisms leads to formation of the various displacement patterns. It should be noted that since the interfacial friction between the granular medium and the cell plates is a stabilizing mechanism, the effect of the interfacial friction is ignored here as similarly argued in Ref. [6].

The existence of these displacement regimes may also be explained by considering three characteristic times involved in the process; namely, the characteristic times t_i and t_d associated with fluid injection and hydromechanical coupling, and the retardation time t_r of the granular medium, assuming the medium can be treated as a nonlinear viscoelastic-plastic solid. The injection time scale may be expressed as $t_i = \ell/v$, where ℓ is a characteristic length of the injection process. The diffusion time scale from hydromechanical coupling may be expressed as $t_d = \eta\ell^2/Ek$, where E is the Young's modulus and k the intrinsic permeability. The retardation time of the medium may be written as $t_r = \eta'/E$, where η' is the apparent viscosity of the granular medium. Two dimensionless times can therefore be defined for this coupled displacement process, i.e., $\tau_1 = t_d/t_i = \eta v\ell/Ek$ and $\tau_2 = t_r/t_i = \eta' v/\ell E$. While the dimensionless time τ_1 determines whether the granular medium response is diffusion governed or deformation governed, the time τ_2 characterizes the viscoelastic response of the granular medium. As τ_2 increases, the material behaviors change from solidlike to fluidlike. The definition of τ_2 is similar to the Deborah number for a viscoelastic fluid.

The displacement regimes can be classified based on the dimensionless times τ_1 and τ_2. Since the fluidlike response occurs when $v\eta$ is the largest in Fig. 1, it is reasonable to assume $t_d < t_r$ or $\tau_1 < \tau_2$. Denote the critical values τ_d and τ_r ($\tau_d < \tau_r$) as the dimensionless times corresponding to the transitions in the granular medium response from diffusion governed to deformation governed and from solidlike to fluidlike, respectively. The injection process is grain displacement dominated if $\tau_d \ll \tau_1 < \tau_2 \ll \tau_r$, and viscous fingering dominated if $\tau_2 \gg \tau_r$. When $\tau_1 \ll \tau_d$, the injection process is governed by diffusion. The experiments shown in Fig. 1 suggest that there exists a threshold value τ_0 ($\tau_0 < \tau_d$) associated with the growth condition. When $\tau_1 < \tau_0$, given the observation time scale and the experimental setup, e.g., the boundary conditions, the growth condition is either not yet met or the growth of the fingers is negligible. The condition, $\tau_1 < \tau_0$, therefore corresponds to the simple radial flow regime and $\tau_0 < \tau_1 \ll \tau_d$ the infiltration-dominated regime. The growth scenario in Fig. 2(a), showing cavity expansion prior to the development of granular fingers, suggests that the growth condition at $\tau_1 = \tau_0$ depends on both the local pore pressure as shown in Ref. [6] and the pore pressure gradient. A schematic for the classification of the displacement regimes based on the characteristic times is shown in Fig. 3.

The variations of the global features as functions of the dimensionless time τ_1 are now examined. In the scaling of τ_1, we may choose the inlet diameter D_i as the characteristic length ℓ. The small strain modulus of Ottawa F110 sand, measured from triaxial compression tests at an effective confining stress of 100 kPa, is $E = 66.2$ MPa. The permeability measured from a flexible wall permeameter is $k = 749$ mD at a confining stress of 137.9 kPa according to the ASTM standard D5084. The modulus and the permeability obtained here serve only as indices since these properties are stress dependent. It should also be noted that since the samples in the triaxial compression and permeability tests are compacted by tampering only, the grain fractions of these samples may be slightly lower than the dense packing in the Hele-Shaw cell.

Denote λ_t as the ratio between the area of the granular fingers and the area enclosed by the infiltration front, both measured from the images at a given time. As shown in Fig. 2(d), where the area ratio λ_t is normalized by its late time average λ, at relatively small τ_1 (tests A2 and B3), λ_t increases at early time but decreases with time as τ_1 becomes large (test C4). Dependence of the early time behaviors on τ_1 suggest that in the transient period, the

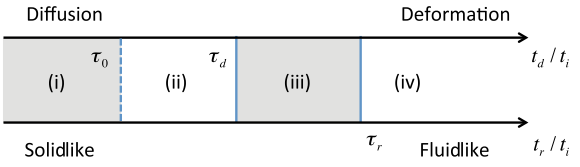

FIG. 3 (color online). Classification of the displacement regimes based on the characteristic times $\tau_1 = t_d/t_i$ and $\tau_2 = t_r/t_i$; (i) the simple radial flow regime, (ii) the infiltration-dominated regime, (iii) the grain displacement-dominated regime, and (iv) the viscous fingering-dominated regime.

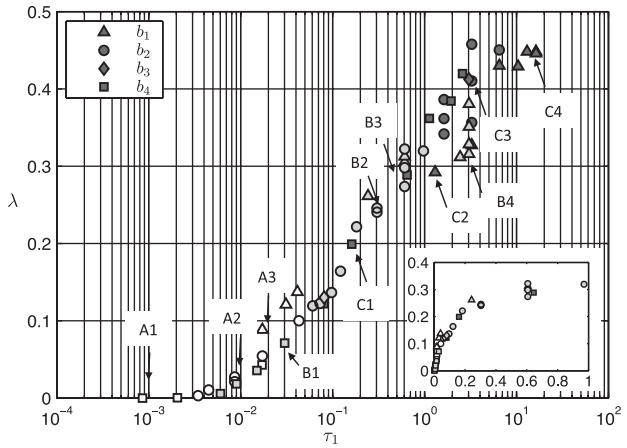

FIG. 4. Variation of the area ratio λ as a function of the dimensionless time τ_1. The marker shape corresponds to the cell gap size: $b_1 = 0.787$ mm, $b_2 = 1.575$ mm, $b_3 = 2.362$ mm, and $b_4 = 3.175$ mm; and the marker color indicates the fluid type: white corresponding to the 50% solution, light gray 90%, and dark gray 100%. Linear scale plot in the inset.

rate of infiltration differs from the rate of cavity expansion or finger growth. As the injection continues, the growth becomes nearly steady state.

Figure 4 shows the area ratio λ, i.e., the late time average of λ_t, as a function of the dimensionless time τ_1. The results suggest that when $\tau_1 < 6 \times 10^{-3}$, growth of granular fingers may be considered negligible. When $\tau_1 > 3$, λ remains approximately constant at $\lambda \simeq 45\%$. We can also observe that at relatively small τ_1 ($\tau_1 < 0.1$), the ratio λ increases nearly linearly with τ_1. The threshold values defining the transitions of displacement regimes may therefore be determined as follows: $\tau_0 = 6 \times 10^{-3}$, $\tau_d = 0.1$, and $\tau_r = 3\eta' k/\eta \ell^2$ (or $\tau_1 = 3$). Since fluid invades ahead of the granular fingers in all the tests here, the apparent viscosity for a fluid and grain mixture may be expressed as $\eta' = \eta f(\phi)$, where $f(\phi)$ is a function of the grain volume fraction ϕ of the mixture and $f(\phi) \gg 1$ for dense granular packing. Consequently, the critical time τ_r reduces to $\tau_r = 3f(\phi)k/\ell^2$.

In addition, the transition from the grain displacement-dominated regime to the viscous fingering-dominated regime around $\tau_1 = 3$ can also be identified from the fractal dimension of the fingers as a function of τ_1. When $6 \times 10^{-3} < \tau_1 < 3$, the fractal dimension D is mostly scattered between 1.70 and 1.80 with an overall gradual decreasing trend. However, when $\tau_1 > 3$, the results show a distinct plateau around $D \simeq 1.64$.

Among the 58 tests, some are repeated tests and some are tests at the same τ_1 but with different combinations of the viscosity η, the injection rate Q, and the gap size b. As shown in Fig. 4, those results at the same τ_1 show good agreement in general, an indication that in these experiments, the area ratio λ is not significantly affected by factors such as the rigidity (or the gap size) of the Hele-Shaw cell, though deflection of the cell plates, in addition to local compaction and displacement of the lateral boundaries, is a mechanism to accommodate the grain displacements. However, the results are scattered when $\tau_1 \simeq 3$. A possible explanation is that around $\tau_1 \simeq 3$, growth of the granular fingers is sensitive to the local grain arrangement. As a result, the patterns are not well developed (e.g., tests B4 and C3).

In summary, we have studied experimentally the coupled displacement process when an aqueous glycerin solution is injected into a dry dense granular medium in a radial Hele-Shaw cell. Depending on the invading fluid viscosity and the injection velocity, fluid flow exhibits a transition from infiltration-governed to infiltration-limited behaviors while the granular medium response displays a transition from that of a rigid porous medium to being fluidlike. Four distinct fluid-grain displacement regimes can be observed from the experiments. These displacement patterns may be classified based on the characteristic times associated with fluid injection, hydromechanical coupling, and viscoelastic plasticity. The threshold values that define the transitions between the displacement regimes can be determined from the variations of the global features as functions of the dimensionless time τ_1.

Acknowledgment is made to the donors of the American Chemical Society Petroleum Research Fund and to the Sand Control Client Advisory Board of Schlumberger for support of this research.

[1] P. G. Saffman and G. Taylor, Proc. R. Soc. A **245**, 312 (1958).
[2] J. Bear, *Dynamics of Fluids in Porous Media* (Dover, New York, 1972).
[3] G. M. Homsy, Ann. Rev. Fluid Mech. **19**, 271 (1987).
[4] R. Lenormand, Proc. R. Soc. A **423**, 159 (1989).
[5] H. van Damme, E. Lemaire, Y. O. M. Abdelhaye, A. Mourchid, and P. Levitz, in *Non-Linearity and Breakdown in Soft Condensed Matter*, Lecture Notes in Physics, edited by K. Bardhan, B. Chakrabarti, and A. Hansen (Springer-Verlag, Berlin, 1993).
[6] O. Johnsen, R. Toussaint, K. J. Maloy, and E. G. Flekkoy, Phys. Rev. E **74**, 011301 (2006).
[7] O. Johnsen, R. Toussaint, K. J. Maloy, E. G. Flekkoy, and J. Schmittbuhl, Phys. Rev. E **77**, 011301 (2008).
[8] X. Cheng, L. Xu, A. Patterson, H. Jaeger, and S. Nagel, Nature Phys. **4**, 234 (2008).
[9] B. Sandnes, E. G. Flekkoy, H. A. Knudsen, K. J. Maloy, and H. See, Nat. Commun. **2**, 1 (2011).
[10] J. G. Speight, *Lange's Handbook of Chemistry* (McGraw-Hill, New York, 2005).
[11] T. A. Witten, Jr. and L. M. Sander, Phys. Rev. Lett. **47**, 1400 (1981).